Cell mechanosensing is regulated by substrate strain energy rather than stiffness

Valeria Panzetta[a], Sabato Fusco[a,1], and Paolo A. Netti[a,b]

[a]Centro di Ricerca Interdipartimentale sui Biomateriali, Università degli Studi di Napoli Federico II, 80125 Napoli, Italy; and [b]Centre for Advanced Biomaterial for Health Care, Istituto Italiano di Tecnologia, 80125 Napoli, Italy

Edited by Rakesh K. Jain, Massachusetts General Hospital, Boston, MA, and approved September 9, 2019 (received for review March 18, 2019)

The ability of cells to perceive the mechanical identity of extracellular matrix, generally known as mechanosensing, is generally depicted as a consequence of an intricate balance between pulling forces actuated by the actin fibers on the adhesion plaques and the mechanical reaction of the supporting material. However, whether the cell is sensitive to the stiffness or to the energy required to deform the material remains unclear. To address this important issue, here the cytoskeleton mechanics of BALB/3T3 and MC3T3 cells seeded on linearly elastic substrates under different levels of deformation were studied. In particular, the effect of prestrain on cell mechanics was evaluated by seeding cells both on substrates with no prestrain and on substrates with different levels of prestrain. Results indicated that cells recognize the existence of prestrain, exhibiting a stiffer cytoskeleton on stretched material compared to cells seeded on unstretched substrate. Cytoskeleton mechanics of cells seeded on stretched material were, in addition, comparable to those measured after the stretching of the substrate and cells together to the same level of deformation. This observation clearly suggests that cell mechanosensing is not mediated only by the stiffness of the substrate, as widely assumed in the literature, but also by the deformation energy associated with the substrate. Indeed, the clutch model, based on the exclusive dependence of cell mechanics upon substrate stiffness, fails to describe our experimental results. By modifying the clutch model equations to incorporate the dependence on the strain energy, we were able to correctly interpret the experimental evidence.

mechanobiology | cell mechanosensing | strain energy | prestrain

Duality of force/deformation sensing is a long-lasting debate in the field of mechanobiology. Indeed physical cues such as forces and deformations produced as a consequence of biunivocal interaction between cells and morphophysical features of their microenvironment are critical for the control of the cell mechanics (1–5). In particular, cell mechanical state depends on 1) the ability to generate forces through actomyosin machinery, 2) the sites where the forces are transmitted externally, and 3) the intracellular environment where forces are applied. Likewise, when a solicitation is generated externally to the cell, the extracellular matrix (ECM), the adhesion sites, and cytoskeleton are involved in reverse order to modify the mechanics of the cell. In particular, the transmission of forces from the inside (cytoskeleton) to the outside (ECM) of cell, and vice versa, are mediated by focal adhesions (FAs) and stretch-sensitive membrane ion channels (6, 7). The FAs are complexes of integrins and other proteins and are considered pivotal structures regulating mechanosensing (8). According to this viewpoint, cells sense substrate mechanical properties—elastic (9) or viscoelastic (10)—by gauging resistance to the traction forces the cells exert on the substrate thanks to the FAs which trigger the assembly of signaling complexes and activate biochemical activities. Then, the molecular connections between FAs, cytoskeletal filaments, and nucleus, to which tensional forces are transmitted (11), endow a discrete path for mechanical signal transfer throughout living cells, but in particular a mechanism to provide tensional stability. Indeed, when cells are subjected to mechanical forces they adopt a mechanoprotective and adaptative behavior, mechanically explained through a strain-stiffening process, to control membrane integrity, cell shape, and structural integrity. In fact, much evidence suggests the cell's ability to develop preserving mechanisms is mediated by the recruitment of submembranous proteins which reinforce the plasma membrane (12–14) or by cytoskeleton structuration (15–19).

Mechanosensing is an intricate and fascinating cellular mechanism that mediates and controls the epigenetic state of the cells (20) and it is at the foundation of the new field of mechanomedicine (21). However, albeit extremely relevant, the underpinning mechanism that drives the inside-out and outside-in cell mechanosensing response is still unclear. The current debate focuses on the biophysical entity that FAs are able to sense, force or deformation (stress or strain), and along this issue several experimental and modeling studies have emerged in the literature (22–24). Perhaps the clutch molecular model is the most eminent modeling approach used to describe cell cytoskeleton dynamics (25) and, more recently, also used to shed light on the basis of the cell mechanosensing mechanism (26–29). However, the concealed constitutive hypothesis of the clutch model is that FAs dynamics depend exclusively upon the stiffness, or the force necessary to induce the deformation, of the ECM. This hypothesis also represents the major limit to the potentiality of the model to depict the effect of mechanical microenvironmental conditions in the presence of residual stress in the ECM. Indeed, the original formulation of the clutch model does not account for the contribution of frozen stresses within the ECM on FA dynamics, which, on the contrary, could have a relevant effect on cell

Significance

In the long-lasting debate about the duality of the force/deformation cell sensing mechanism we focused attention on the question of whether the cell is sensitive to the stiffness or to the energy required to deform the surrounding material. To address the role of strain energy as a regulator of cell mechanosensing we investigated the cytoskeleton mechanics of cells seeded on linearly elastic substrates, applying several levels of deformation before and after cell seeding. The results indicated that cells recognize the prestrain, exhibiting a stiffer cytoskeleton on stretched material compared to cells seeded on unstretched substrate. This observation clearly suggests that cell mechanosensing is not mediated only by the stiffness but also by the deformation energy of the substrate.

Author contributions: S.F. and P.A.N. designed research; V.P. and S.F. performed research; V.P. analyzed data; and V.P., S.F., and P.A.N. wrote the paper.

The authors declare no competing interest.

This article is a PNAS Direct Submission.

See Commentary on page 21960.

[1]To whom correspondence may be addressed. Email: sabfusco@unina.it.

This article contains supporting information online at www.pnas.org/lookup/suppl/doi:10.1073/pnas.1904660116/-/DCSupplemental.

First published September 30, 2019.

mechanics and functions. Residual stresses are ubiquitous in native tissues and their role is deemed central in tissue morphogenesis, growth, homeostasis, and function (30–32), pointing to the hypothesis that the cell mechanosensing mechanism would rely on the energy of deformation of the substrate rather than upon the sole stiffness.

To assess this important issue, here cells were cultured on substrate with different levels of frozen stresses and mechanical features of the cytoskeleton were measured to gain insight on the mechanosensing regulator mechanism. In particular, the mechanical state of murine fibroblasts BALB/3T3 and murine preosteoblast MC3T3 has been sampled at different time points, before and after the stretching application. Particle tracking microrheology (PTM) was the technique used to investigate the heterogeneous spatial distribution and the time evolution of cell stiffness under culture condition (33, 34). Furthermore, cells were subjected via elastic substrates to different levels of uniaxial deformation: 0%, 6%, and 9% for polydimethylsiloxane (PDMS) and 0% and 9% for polyurethane (PU). Cell stiffness modulating responses to deformations are obtained and discussed. In particular, the mechanical response of cells was sampled immediately after the deformation and after 2 h, when the processes of remodeling associated with the mechanical stimulus and involving the cytoskeleton can be considered partially/totally transduced by cells. We confirmed the stiffening behavior of cells depending on the amplitude of the stimulus. Furthermore, congruent mechanical behaviors were found for cells seeded on substrates previously stretched to the same levels of deformation. This process, which may represent an increase of cell prestress and a mechanism adopted by cells to be prepared to successive or repetitive mechanical stimuli, also directs the mechanism of mechanical recognition of physical environment toward the cell's ability to sense the strain energy stored in the substrate. Under this hypothesis, the clutch molecular model has been adopted to simulate the cell response in the particular case of substrate with a given prestrain. The fact that the simulations were in accordance with experimental results only in the case of model modification by the addition of a factor addressing the strain energy of the substrate has represented the starting point for the discussion about the dual mechanism of mechanosensing. The evidence found, pinpointing a primitive quantity such energy of deformation (with respect of force/deformation) as new cell mechanosensing entity, could further contribute to transcend the current debate.

Results and Discussion

Cell Mechanics and Sensing of Strain Energy. Nowadays it is well known that cells are able to respond to mechanical cues and, in particular, to adapt their morphology, cytoskeletal structure, and mechanical properties to the stiffness of their environment. Nevertheless, the debate on whether cells sense force or deformation on an elastic substrate is still open. Here, we tried to understand if cells are able to sense not only environmental stiffness, but, in particular, the energy stored in the ECM when prestreched. To respond to this question, we seeded 2 different cell lines (BALB/3T3 and MC3T3) on 2 linear elastic substrates (stiffnesses of 1 MPa and 0.6 MPa), which were stretched to 3 different levels of deformation (0%, 6%, and 9%) before the cell culture. The levels of deformation were chosen on the basis of 2 different considerations. First, they are in the linear regime of the stress–strain curve of the PDMS and the PU, in order to avoid a nonlinear strain-stiffening for the materials (*SI Appendix*, Fig. S1). Second, in view of the experiments in which the deformations were applied when the cells were already attached to the substrate, they were low enough not to cause damage to the cells from a morphological point of view. In fact, as already reported by Mizutani et al. (35), under the chosen levels of deformation the cells are not disassembled, but they still appear to be tensile. On the contrary, degrees of deformation greater than 15% almost instantly destroyed the cells.

Cell mechanical characterization was conducted by particle tracking experiments for the 3 different levels of deformation (0%, 6%, and 9%). The mechanical characterization for the null deformation defines the base-mechanical state of fibroblasts and preosteoblasts. The mean squared displacements (MSDs) of the freely moving nanoparticles embedded in cells give information about the resistance to motion posed by the cytoplasm and, in an indirect way, about the mechanics of the cell microenvironment (*Materials and Methods*). The stretching chamber and the procedure of stretching are illustrated in Figs. 1 and 2, *A.1* and *SI Appendix*, Fig. S2, respectively. We compared the MSDs of naoparticles embedded in control cells with those of naoparticles in the cells cultured on stretched substrate. As shown in Fig. 2, *A.2*, when both cell lines investigated are cultured on PDMS substrates with levels of deformation of 6% and 9%, the amplitude of MSDs decreased, resulting about 1.2/1.5-fold (6% deformation, see Table 1 for statistical information) and 1.7/1.8-fold (9% deformation, Table 1) lower than in control condition at all time lags explored. The effectiveness of deformation was also confirmed by the significant reduction of the radius of gyration (*SI Appendix*, Fig. S3 and Table S1) and by atomic force microscopy cell mechanical characterization reported for 9% of deformation in *SI Appendix*, Fig. S10. The observed reduced motion of nanobeads, omitting the active contribution of actin flow rate, could be associated with an augmented hindrance and a reduction of the characteristic mesh size of the actin network. This leads to a more polymerized cytoskeleton (Figs. 2 and 3*A* and Table 1) and consequently to a progressive increase of the stiffness passing from 0% to 9% of applied deformation. Similar results have been obtained by using PU as a substrate for both cell lines (Figs. 3*B* and 4, Table 2, and *SI Appendix*, Fig. S3 and Table S2). PU has stiffness comparable to PDMS and cell-stretching results were almost overlapping on these 2 different substrates. Furthermore, experiments on polyacrylamide with a stiffness significantly lower (30 kPa) were conducted. Trends, reported in *SI Appendix*, Fig. S4, were confirmed also on hydrogel-like materials with low stiffness. As reported in *Materials and Methods*, all of the stretching tests were conducted on substrates (PDMS and PU) incubated with cell culture medium for 1 h at 37 °C to promote protein adsorption. In order to control any kind of interference of stretching on the superficial layer of absorbed

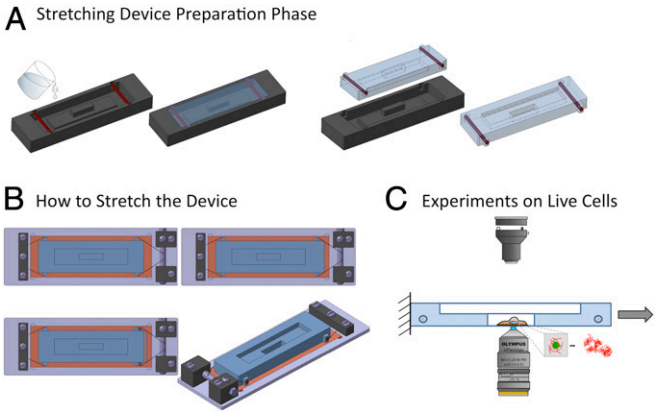

Fig. 1. (*A*) Stretching device preparation. The prepolymers of PDMS and PU were mixed and degassed under vacuum and cured at high temperature. Finally, the stretching device was removed from the master. (*B*) The deformation is applied by rolling an iron wire attached to the unconstrained side of the chamber around a stainless steel bar. (*C*) Cells are cultured on the devices and PTM experiments are performed.

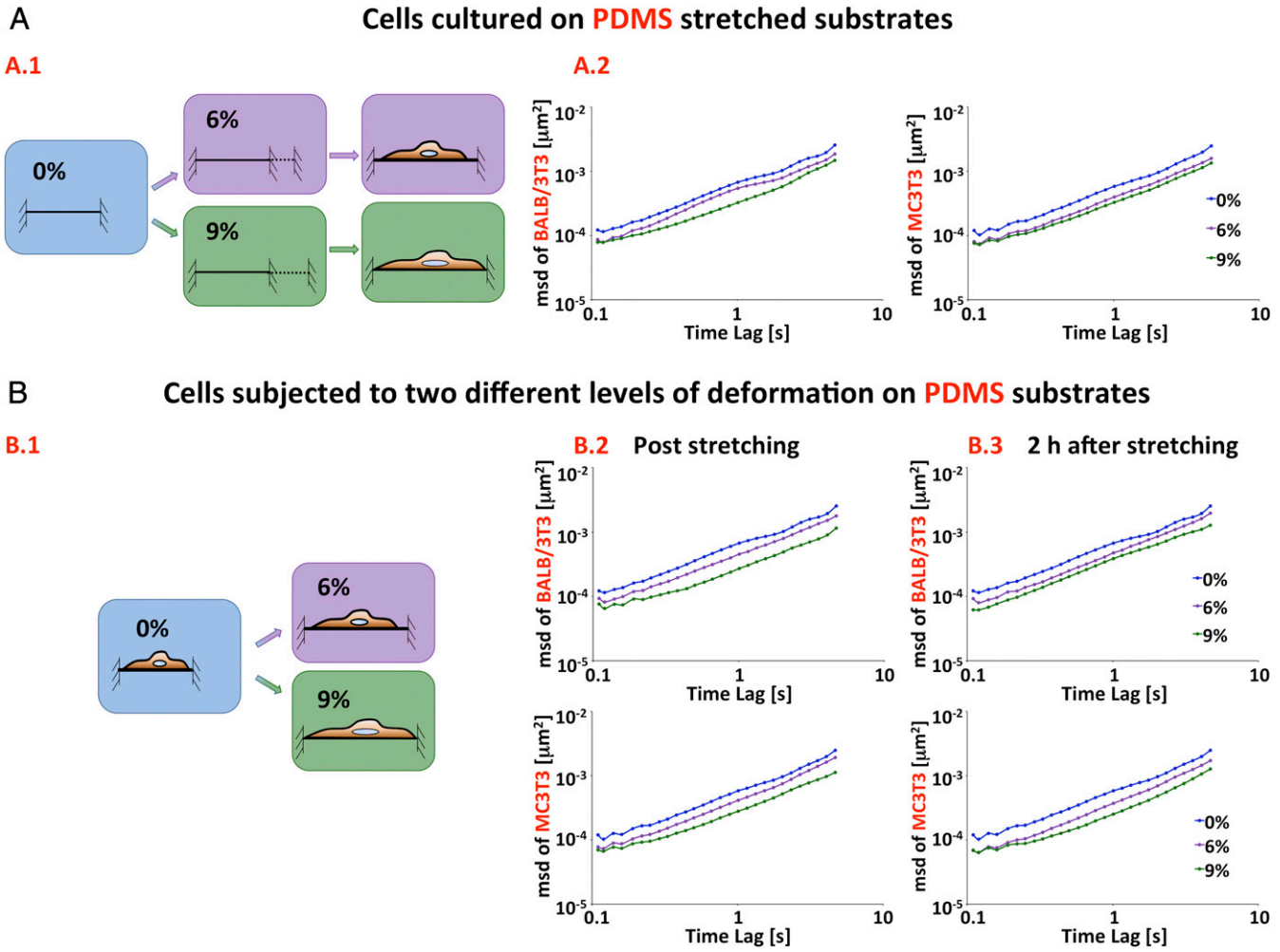

Fig. 2. Schematic representations of the experimental setup of the stretching experiments. Devices were stretched to a final deformation of 6% and 9% and then the cells were cultured and allowed to attach to the stretched substrates (*A.1*); the cells were cultured on the unstretched devices and successively subjected to 2 different levels of deformations (*B.1*). Ensemble-averaged MSDs of 500-nm fluorescent particles in BALB/3T3 and MC3T3 cells cultured on stretched PDMS devices (*A.2*) and subjected to different levels of uniaxial deformation (0%, 6%, and 9%) immediately after the deformation (*B.2*) and 2 h after the deformation (*B.3*). $n > 100$ for all studied cases.

proteins (i.e., desorption or conformational changes), further experiments were made on PDMS substrate chemically decorated by RGD peptides. Moreover, cell mechanical characterizations on unstretched and stetched PDMS were made in serum-free conditions to directly promote cell adhesion on RGD peptides. Results, reported in *SI Appendix*, Fig. S5, were in good agreement and confirmed those obtained on substrates not chemically functionalized (Figs. 2 and 3*A*).

This evidence suggested that a more intriguing and energy-driven sensing mechanism of mechanical signals was adopted by cells: adhesive cells are able to sense, together with the mechanical properties (elasticity and viscosity) of the external microenvironment, the mechanical history of the substrate by sensing the energy stored when deformed. Cell recognition strain energy instead of stiffness might also explain the regulatory function of residual stresses in native 3-dimensional tissues. Indeed, many observations have revealed their existence, even in the absence of external loads, in many tissues and organs such as blood vessels, heart valves, cartilage, skin, brain, and solid tumors (30–32). The presence of residual stress in tissues can be recognized by cells' mechanosensing only if this mechanism is based on strain energy rather than stiffness. From this point of view, discussed experiments can be interpreted as an in vitro emulation of such residual stress and the results obtained as the ability of the cell to perceive them, in addition to the intrinsic mechanical properties of the ECM.

Equivalence on Cell Mechanics of Strain Energy Application before and after Cell Seeding and Its Reversibility. The comparison of the mechanical responses of fibroblasts (BALB/3T3) and pre-osteoblasts (MC3T3) attached to stretched PDMS and PU substrates with that of the same cells attached to unstretched substrates and successively stretched was also performed. The procedure of stretching is illustrated in Fig. 2, *B.1*. In this case, the particle tracking experiments were conducted at 3 different time points: 1) before the stretching of the substrate to evaluate the basal mechanical state (same conditions of 0% as in the previous experiment), 2) immediately after the mechanical stretching to capture the cellular elastic response to the deformation, and 3) 2 h after the stretching to determine the new mechanical state of the cell excluding transient effect and cage effect in bead motion tracking due to the stretching.

Fig. 2*B* and Fig. 4*B* show a dramatic effect on the dynamics of the tracer beads when the cells are subjected to increasing levels of deformations for both cell lines and substrates investigated. In the particular case of PDMS substrate, where intermediate

Table 1. Statistical comparison of the data collected on PDMS devices

	6%			9%		
	On stretched devices	After stretching	2 h after stretching	On stretched devices	After stretching	2 h after stretching
0%	***, ##	***, ##	***, ###	***, ###	***, ###	***, ###
6%						
On stretched devices		NS, NS	NS, NS	**, ###	***, ###	***, ###
After stretching			NS, NS	***, ###	***, ###	***, ###
2 h after stretching				***, #	***, ###	***, ###
9%						
On stretched devices					*, #	NS, ###
After stretching						*, NS

Asterisks (*) refer to MSDs of nanoparticles inside the BALB/3T3 cells at $\tau = 1$ s and hash signs (#) to those of nanoparticles inside MC3T3 cells. ***, ### $P < 0.001$; **, ## $P < 0.01$; *, # $P < 0.05$; NS, not significant.

levels of deformation were considered, passing from unstretched sample to 6% and 9% levels of deformation, the MSD amplitude decreased, respectively, about 1.5/1.3-fold and 2.5/2.1-fold lower than in the control condition at all explored time lags (Figs. 2 and 3). Also in this case we measured a significant reduction of the radius of gyration immediately after the application of the deformation (*SI Appendix*, Fig. S3 and Table 1). A threshold effect on the ability of cells to sense and respond to mechanical deformation was observed: The MSDs are substantially unaltered when the deformation applied is equal to 3% (the MSD curves of 0% and 3% deformation present a good overlap; *SI Appendix*, Fig. S6), indicating that this degree of deformation does not induce sensitive variations in the intracellular mechanics.

The cell strengthening process due to 6% deformation was maintained up to 2 h after the application of the mechanical stimulus. In fact, the MSDs remained essentially unchanged during the 2 h after substrate stretching and lower than those measured in the control condition (Fig. 2). Similar behavior was exhibited by MC3T3 cells when subjected to 9% level of deformation. In the case of BALB/3T3 cells, the strong decrease of MSDs and radius of gyration due to 9% deformation was followed 2 h after by a progressive increase of both parameters, indicating a relaxation of mechanical state occurring after the stretching. Anyway, the MSDs and the radius of gyration continued to be significantly smaller than those measured in control unstretched condition and lower than those of beads in cells stretched to 6% deformation. A similar result was observed when the final 9% deformation was obtained in a double-step process. In this experiment, to evaluate if cells are effectively able to support successive mechanical stimuli, 2 h after the application of 6% deformation an additional deformation taking to a final 9% deformation was imposed on cells. Interestingly, 2 h after the second deformation (4 h from the beginning of the experiment) the MSD amplitude resulted to be closer than those of nanobeads in cells exposed directly to 9% deformation (Fig. 5), indicating that cell stiffening promoted by the mechanical stretch of the substrate is independent from the process by which the final deformation stage was reached. These results suggest that, at least for this cell type and for the specific stimulus, the mechanical internal energy of cells is a state quantity, depending on the state and not on the path by which the process has occurred (Fig. 5).

Effects of Strain Energy Sensing on Cell Morphology. We evaluated the effects of the mechanical stimuli after 2 h from the application of 6% and 9% levels of PDMS deformation on BALB/3T3 and MC3T3 spreading areas (Fig. 6 and *SI Appendix*, Figs. S7 and S8). As already reported in the literature (36, 37), also here we report an increase of cell spreading areas passing from unstretched to stretched substrate. In particular, the average values of the cell spreading area was slightly dependent ($P < 0.05$) on the intensity of the final deformation state (6% or 9%) for both BALB/3T3 and MC3T3 cells. Similar behavior was found evaluating the effect of mechanical stretching on the cell shape factor (minor axis/major axis). On BALB/3T3 cells, usually characterized by typical spindle-like shape, 6% and 9% levels of deformation induced a slight decrease of the shape factor (more

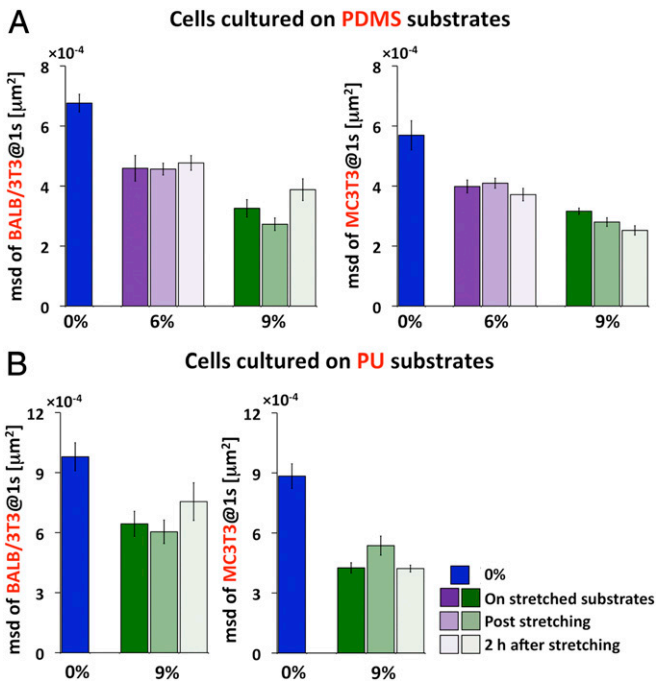

Fig. 3. Data related to MSDs of nanoparticles inside BALB/3T3 (*Left*) and MC3T3 (*Right*) cells at $\tau = 1$ s on PDMS (*A*) and PU (*B*) substrates are presented as mean ± SEM, $n > 100$ for all studied cases. Statistical analysis is reported in detail in Table 1.

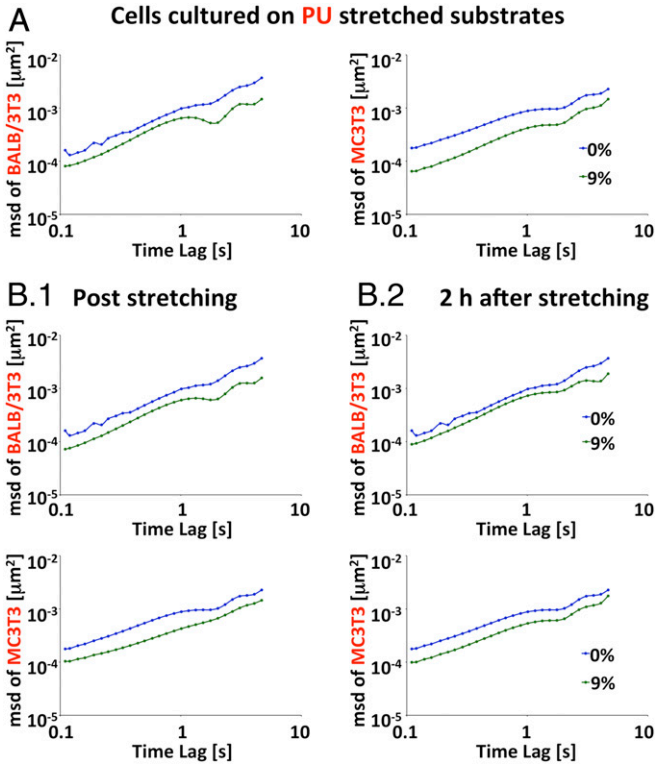

Fig. 4. Ensemble-averaged MSDs of 500 nm fluorescent particles in BALB/3T3 and MC3T3 cells cultured on stretched PU devices (*A*) and subjected to different levels of uniaxial deformation (0% and 9%) immediately after the deformation (*B.1*) and 2 h after the deformation (*B.2*). $n > 100$ for all studied cases.

significant for 6% deformation), indicating a more elongated shape (Fig. 6 *B–C* and *H*). Conversely, on MC3T3, generally characterized by well-spread cell body, applied deformation led to an increase of the shape factor toward more rounded cells (Fig. 6 *E*, *F*, and *K*). For both cell lines no statistical difference was found between the values distribution of 6% and 9%. At the same time, orientation and alignment for MC3T3 on both substrates before and after deformation of 0% and 9% were measured (*SI Appendix*, Fig. S9*A*). In all cases, substrate stretching did not affect cell alignment and/or orientation. Similar trends were also observed on PU substrates (*SI Appendix*, Fig. S9*B*).

It is well known that biophysical properties of cells and their mechanical state can be modulated by tuning the physical properties of the ECM and this relationship is often discussed in terms of morphological features of cells such as spreading and shaping. On the other hand, our results, even if they partly corroborate this vision, indicate clearly that cell mechanical state and morphological parameters such as spreading area and shape factor are not in a continuous and direct relationship with the intensity of the deformation, at least at the equilibrium stage (after 2 h from the application of the mechanical stimulus). The relationship between biophysical properties of cells and intensity of the stimulus, rather, appears to be discrete, even if we have no knowledge on what happens between 3% and 6% of deformation (*SI Appendix*, Fig. S2). The rapid response in terms of cellular stiffness, induced by the mechanical stimulus in the cases of 6% and 9% of deformation, can be attributed to the elastic modulus of the cytoskeletal networks, consisting of filamentous actin and actin-binding proteins, such as myosin II and filamin. The application of an external mechanical stimulus can induce cascading effects starting from the increase of tensional state in stress fiber, followed by the consequent growth of their cross-sectional area and FA size increase. As previously demonstrated, the dimension of these 2 structures controls the mechanical properties of the FA–stress fiber complex, which mediates the transmission of forces internally, and consequently of the overall cytoskeletal structure (33, 38).

Furthermore, the physical connection between the nucleus and the ECM and the other cells is mediated by the cytoskeleton and realized by LINK (Linker of Nucleoskeleton and Cytoskeleton) complex proteins. This intimate communication explains the ability of biophysical cues to distort the nuclear envelope and generate biochemical responses. In particular, it has been demonstrated that that there is a direct relationship between ECM stiffness and nuclear area. The generation of cellular tension on stiff substrates leads to increased nuclear area and condensed chromatin. Considering that, as previously shown, the mechanical tension of stretched cells is increased for 6% and 9% deformations, we have evaluated the effects of them on nuclear area. As expected and similarly to the spreading, we found that the nuclear area increased as a consequence of the mechanical stimuli (Fig. 6 *I* and *L* and *SI Appendix*, Fig. S7 for PDMS; Fig. 7 *G* and *I* and *SI Appendix*, Fig. S8 for PU). The structural plasticity of cytoskeleton and nucleus are profoundly related: If initially the cytoskeletal tension is responsible for the increased condensation and stiffness of nucleus, we believe that the consequent altered nuclear status initiates changes in signaling pathways and in synthesis and localization of cytoskeleton proteins. As a consequence, the stiffening we found after 2 h from the application of 6% and 9% levels of deformation could be related to this nuclear mechanotransduction process (39).

Putting together the above discussion and evidence about the deformation experiment, it is possible to hypothesize different molecular paths activation for the assembly of cytoskeleton in response to active mechanical stimuli (external stretching) and biophysical characteristic of the microenvironment that are both based on a dual nature of cell–material cross-talk through a force and deformation mechanosensing process. To better describe this mechanism, we implemented a modified clutch model in which the first experimental condition (cells cultured on stretched substrates) was simulated.

Stretched Substrate and the Clutch Model. As discussed previously, fibroblasts cultured on stretched substrates exhibited a stiffening behavior in direct proportion to the levels of applied deformation, reminiscent of the cell response to stiffness on elastic substrates (33, 40, 41). The response of cells to the strain energy of the substrate can be interpreted through the molecular clutch model. The model, as extensively explained in other contexts (27, 29), is able to describe the mechanical cross-talk between the cells and the external environment. In particular, in this model the molecular clutches (integrins and adaptor proteins) connect the ECM to the cell cytoskeleton and guarantee the transmission

Table 2. Statistical comparison of the data collected on PU devices

	9%		
	On stretched devices	After stretching	2 h after stretching
0%	***, ###	***, ###	***, ##
9%			
On stretched devices		NS, #	NS, NS
After stretching			NS, #

Asterisks (*) refer to MSDs of nanoparticles inside the BALB/3T3 cells at $\tau = 1$ s and hash signs (#) to those of nanoparticles inside MC3T3 cells. ***, ### $P < 0.001$; **, ## $P < 0.01$; *, # $P < 0.05$; NS, not significant.

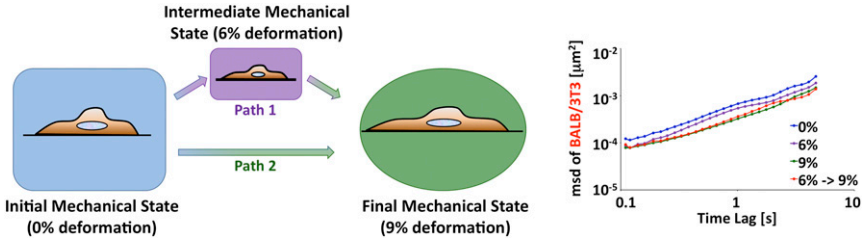

Fig. 5. Ensemble-averaged MSDs of 500-nm fluorescent particles in BALB/3T3 cells in control condition (blue curve) and subjected to 9% uniaxial deformation administered in a single shot (green curve acquired immediately after the deformation) or in 2 consecutive mechanical stimuli (red curve acquired 4 h after the first deformation). $n > 100$ for all studied cases.

of forces from the internal to the external side of the cell. The actin flows through the molecular clutches and the myosin motors counterbalance the elastic resistance of the substrate to the deformation, reducing the actin flow and increasing the rate of force loading on the clutches in a stiffness-dependent manner.

Here, we hypothesize that the sensing of the substrate strain energy can happen through a similar mechanism. To test this hypothesis, a modified version of the canonical clutch model (27, 42), in which the substrate was modeled as constituted by 2 linear elastic springs arranged orthogonally (Fig. 8 and *SI Appendix*, Fig. S11), was proposed. The substrate was assumed to be isotropic, then the same value was chosen for the elastic constants of the 2 springs. In this model the orthogonal spring is the element able to take memory of the strain energy stored inside the material, which depends upon the spring constant (held constant during the experiment) and the deformation applied. Eqs. **3**–**13** were solved simultaneously using the MATALB ODE solver ode15s for stiff systems for different values of k_s, n_c, and x_0, which represents the deformation applied to the substrate. As shown

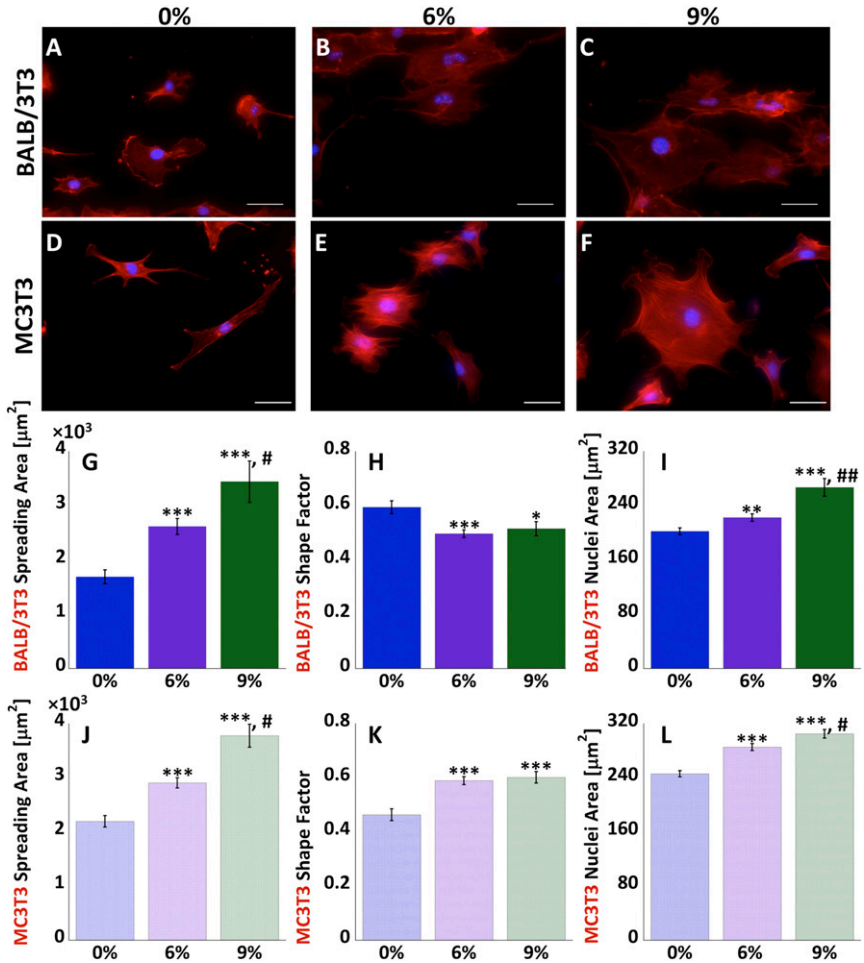

Fig. 6. Representative images of morphology and cell nuclei of BALB/3T3 (*A*–*C*) and MC3T3 (*D*–*F*) cells subjected to different levels of uniaxial PDMS deformation (0%, 6%, and 9%) 2 h after the deformation. The effects of substrate deformation on cell spreading (*G* and *J*), cell shape factor (*H* and *K*), and nuclei area (*I* and *L*). Data were presented as mean ± SEM. $^{*}P < 0.05$, $^{**}P < 0.01$, and $^{***}P < 0.001$ as compared with cells on unstretched devices; $^{\#}P < 0.05$ and $^{\#\#}P < 0.01$ as compared to cells subjected to 6% deformation. (Scale bars, 50 μm.)

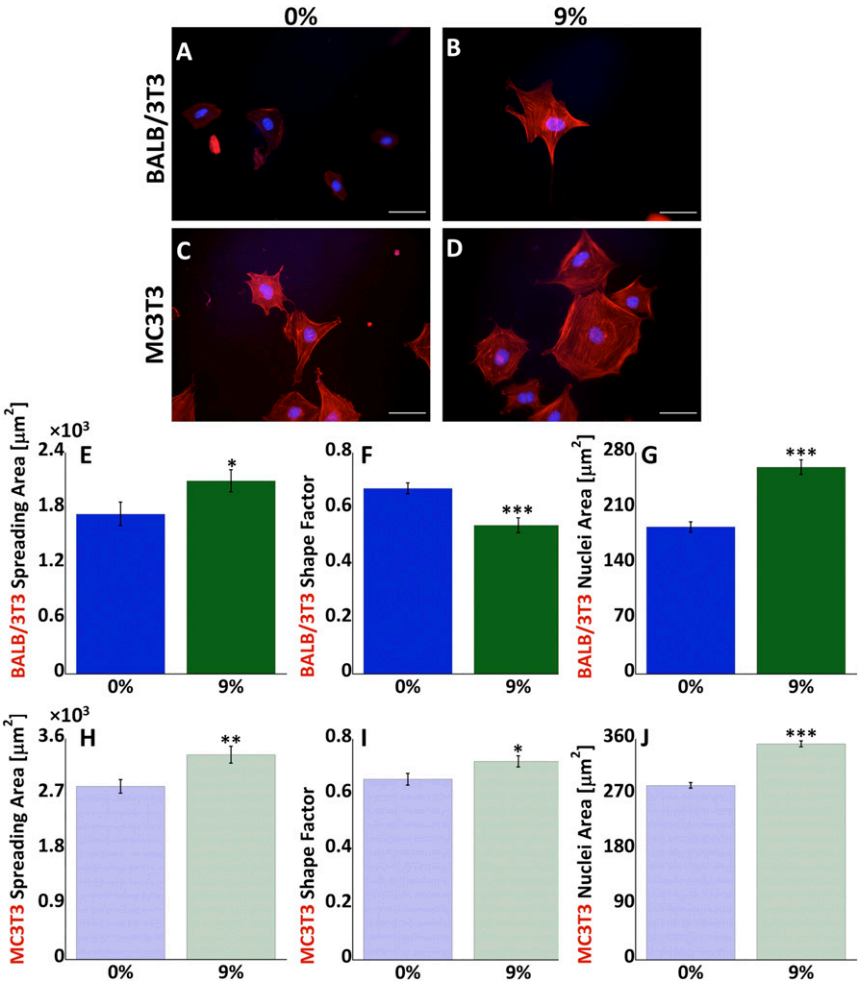

Fig. 7. Representative images of morphology and cell nuclei of BALB/3T3 (*A* and *B*) and MC3T3 (*C* and *D*) cells subjected to different levels of uniaxial PU deformation (0% and 9%) 2 h after the deformation. The effects of substrate deformation on cell spreading (*E* and *H*), cell shape factor (*F* and *I*), and nuclei area (*G* and *J*). Data are presented as mean ± SEM. **P* < 0.05, ***P* < 0.01, and ****P* < 0.001 as compared with cells on unstretched devices. (Scale bars, 50 μm.)

in Fig. 9, the ODE solution captures the behavior observed in our experiments. In particular, optimum stiffness (characterized by the minimum actin flow rate) shifts to lower values when x_0 increases (Fig. 9, *Left*), or, from another point of view, the optimum number of clutches shifts to higher values when x_0 increases (Fig. 9, *Right*). This result indicates that the substrate deformation is interpreted by the cell as an additional stiffness, which requires the involvement of a greater number of clutches to counterbalance the resistance of the substrate, or, in a specular way, on a softer, but stretched substrate the same number of clutches is engaged at level of the FA. As already observed in previous work (33), we know that a direct relationship exists between the length of FA, here represented by the number of clutches, and the mechanical properties of fibroblasts; then we can affirm that the shifting of the number of clutches toward higher values, when the substrate deformation increases, is associated with a reinforcement process and, consequently, with a stiffening of the cell, as observed in Figs. 2 and 3. By implementing the model in its canonical form (*SI Appendix*, Figs. S11–S13 and *Appendix 1*), it was not possible to simulate the behavior of cell on prestreched substrate (*SI Appendix*, Fig. S13). The introduction of an additional element (orthogonal spring), the task of which was to take into account the mechanical history of the material, allows us to interpret nonlinear behaviors such as prestrain, viscoelasticity, or yield stress, still remaining in agreement with the previous formulation of the model (27, 29).

Conclusions

We analyzed the cell's ability to mechanosense a stretched elastic material. To this purpose, cells were seeded both on stretched and unstretched substrates. Because the substrates were made of linear and elastic materials, no changes in their stiffness occurred in the unstretched and stretched states, but surprisingly we found the mechanical states of cells depended upon the degree of stretching. In particular, the mechanical integrity of the cytoskeleton

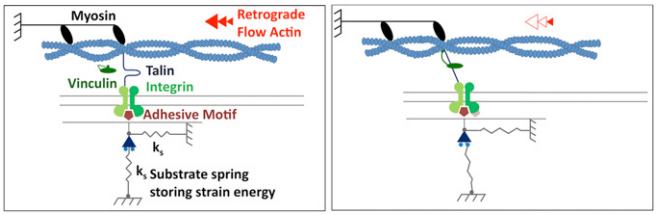

Fig. 8. Motor-clutch model. Molecular myosin motors (black structures) generate retrograde actin flow toward the center of the cell. The molecular clutches connect the actin to the external microenvironment, binding at a constant association rate k_{on} and unbinding at a force-dependent dissociation rate $k^*_{off,i}$. In this version of the clutch model, the substrate is modeled as constituted by 2 linear elastic springs arranged orthogonally.

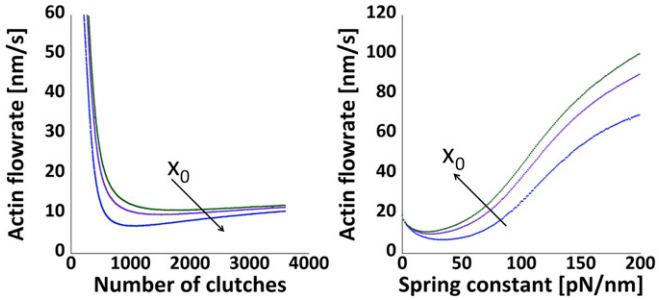

Fig. 9. The optimum number of clutches (characterized by the minimum actin flow rate) shifts to higher values when x_0 increases (*Left*), or, from another point of view, the optimum stiffness shifts to lower values when x_0 increases (*Right*).

of cells seeded on stretched substrates was found to be higher compared to those cells seeded on unstretched substrate and comparable to those of cells stretched together with the substrate. Indeed, cells seeded on substrates with higher deformation energy (stretched) promoted more robust cytoskeleton assembly. This evidence has suggested investigating if the process of mechanosensing could be mediated not only by the substrate stiffness but, in a more generalized way, also by the energy of deformation involved in the cell–material interplay. To this aim, the response of cells to the strain energy of the substrate has been modeled through the molecular clutch model, able to describe the mechanical cross-talk between the cells and the external environment. Thanks to the addition of an extra spring element, we were able to take into account the strain energy stored in the prestreched material, and the simulation trends were in accordance with experimental results.

Materials and Methods

Stretching Device Fabrication. Stretching chambers were fabricated in PDMS and PU. A prepolymer PDMS, purchased from Dow Corning and obtained by mixing the silicon elastomer base and the cross-linking agent at a ratio equal to 10:1, was poured into an aluminum master, degassed under vacuum for 1 h, and cured at 120 °C for 3 h. After having cooled the PDMS mold down to room temperature (RT), the chamber was peeled from the master (Fig. 1).

The PDMS device consists of a transparent bottom (66 × 20 mm^2) with a central window which has a surface of (15 × 4 mm^2, ~220 μm thick), deformable up to 20% along a single direction. The Young's modulus of PDMS is about 1 MPa (*SI Appendix*, Fig. S1) (33, 43, 44). To study the effect of prestrain on an additional material, the PDMS central window was substituted with a PU sheet. The PU sheet was obtained by mixing part A and part B of a bicomponent PU elastomer (F-105 A/B 5 shore; BJB Enterprises) at a ratio equal to 3:1 and curing the elastomer at 80 °C for 3 d. The Young's modulus of PU is about 0.6 MPa (*SI Appendix*, Fig. S1). PU samples were exposed to oxygen plasma for 120 s at a power of 50 W to increase their wettability and favor cell adhesion.

The deformation is applied by rolling an iron wire attached to the unconstrained side of the chamber around a stainless steel bar (*SI Appendix*, Fig. S2 in dark red). The magnitude of deformation was calibrated from the displacement of points marked on the elastic substrate. Uniaxial deformation of the elastic substrate is accompanied by a small degree of subsidiary deformation in the orthogonal direction, because both sides of the elastic substrate are allowed to deform. When the deformation has been applied, it is held constant during the experiments.

In this study, to evaluate the ability of the cells to perceive the substrate deformation, we applied 2 different deformations of 6% and 9% and then we cultured the cells and allowed them to adhere to the surface for about 3 h. We have also evaluated the mechanical response of cells when they were cultured on the unstretched substrates and then subjected to the stretch (6% and 9% deformations and 2 successive deformations, 6 to 9%). The mechanical response of cells in this second kind of experiment was evaluated at 3 different time points: 1) before the mechanical deformation, to define the base-mechanical state of the cells, 2) immediately after the deformation, to measure the elastic response of the cells, and 3) 2 h after the deformation, to measure the mechanical response after eventual relaxation phenomena. During the mechanical stimulation, the cells were maintained at 37 °C in human-humidified air containing 5% CO_2. All devices were autoclaved and then incubated with Dulbecco's modified Eagle's medium (DMEM) supplemented with 10% FBS for 1 h to promote protein adsorption, before cell culture.

Cell Culture. Mechanical stretching and PTM experiments were performed on mouse embryo fibroblasts BALB/3T3 cells and murine osteoblastic MC3T3 cells. BALB/3T3 and MC3T3 cell lines were cultured at 37 °C in 5% CO_2 in a humidified incubator, the first one in DMEM supplemented with 10% FBS (BioWhatter), 2 mM L-glutamine (Sigma), 1,000 U/L penicillin (Sigma), and 100 mg/L streptomycin (Sigma) and the second one in alpha-modified essential medium supplemented with 10% FBS (BioWhatter), 2 mM L-glutamine (Sigma), 1,000 U/L penicillin (Sigma), and 100 mg/L streptomycin (Sigma).

In each experiment, 2×10^3 cells were suspended in 250 μL of cell culture medium and seeded on the central window of the stretching device. The cells were allowed to adhere to the devices for 3 h and 500 μL of cell culture medium were added in the chamber.

PTM. PTM was performed as previously described (34) with slight changes. A ballistic gun (Bio-Rad) was used to deliver fluorescent carboxylate-polystyrene particles (0.500 μm diameter; Invitrogen Molecular Probes) in the cytoplasm of BALB/3T3 and MC3T3 cells. Helium gas at 450 psi was used to shoot nanoparticles within targeted cells and, after bombardment, cells were washed extensively with phosphate-buffered saline (PBS) and allowed to recover for 24 h. Then, the cells were cultured after or before the application of the deformation and allowed to adhere on the substrates for about 3 h. Videos of nanoparticles embedded inside the cells were collected in time lapse for a total of 5 s at 100 frames per s using an inverted fluorescence microscope (Olympus IX81; Olympus) equipped with a 60× water immersion objective with N.A. = 1.20, plus 1.6× magnification of internal microscope lens, and a Hamamatsu ORCA-Flash 2.8 CMOS camera (Hamamatsu). Experiments were performed under physiological conditions, using a microscope stage incubator (Okolab) to keep cells at 37 °C with 5% CO_2. Each deformation was applied at least in 3 different experiments, 20 cells were analyzed for each condition (when the cells were cultured directly on stretched substrate, when the cells were cultured on unstretched substrate before the mechanical deformation, and immediately after the deformation and 2 h after the deformation), and 30 to 50 particles were tracked for each cell.

PTM is a technique used to have indirect information about the local viscoelastic properties of living cells (45–48). By using our self-developed MATLAB 7 code, the trajectories of the nanoparticles were obtained, and then the MSDs were calculated with the following equation:

$$\left\langle \Delta r^2(\tau) = [x(t-\tau) - x(t)]^2 + [y(t-\tau) - y(t)]^2 \right\rangle, \quad [1]$$

where < > angular brackets mean time average, τ is the time scale, and t is the elapsed time.

In addition to the MSD, the radius of gyration (R_g) was calculated as the average distance between all measured positions in a trajectory:

$$R_g^2 = \frac{1}{2N^2} \sum_{i=1}^{N} \sum_{j=1}^{N} \left(\vec{R_i} - \vec{R_j} \right)^2. \quad [2]$$

In the case of living cells, because of the presence of active contributions to the motion of nanoparticles inside the cytoplasm, it is not possible to directly relate the MSDs to the viscoelastic moduli by using the generalized Stokes–Einstein equation. However, MSD and radius of gyration are 2 indicators of the intracellular mechanics and, in particular, it was demonstrated that the MSD amplitude and the local stiffness in cells are inversely proportional (49, 50). MSD and the radius of gyration were used to compare the cell mechanics of BALB/3T3 and MC3T3 cells in each condition analyzed (51).

Cell Adhesion. For cell spreading and orientation analysis, in control conditions and 2 h after the application of deformations of 6% and 9%, BALB/3T3 and MC3T3 cells were fixed with 4% paraformaldehyde for 20 min at RT. The fixed cells were permeabilized with 0.1% Triton X-100 (Sigma-Aldrich) in PBS for 10 min. The actin filaments were stained with TRITC phalloidin (Sigma-Aldrich) in PBS for 30 min at RT. Cell nuclei were stained with DAPI (Sigma-Aldrich). Images of the specimens were taken using an Olympus IX81 inverted microscope and a 20× objective to quantify cell spreading and cell orientation. Fluorescent images were imported into ImageJ software (NIH) for postprocessing analysis and quantification of the cell area. In particular, individual cells were thresholded manually on the basis of the phalloidin

staining, and the spreading area, the orientation, and the shape factor of their thresholded bodies were determined using a custom macro and an ellipse-fitting function in ImageJ.

Clutch Model. The motor-clutch model, as schematized in Fig. 8, was implemented to study the role of substrate stretching on cytoskeleton assembly and mechanics. Briefly, in this model molecular myosin motors generate retrograde actin flow toward the center of the cell. The molecular clutches connect the actin to the external microenvironment, binding at a constant association rate k_{on} and unbinding at a force-dependent dissociation rate $k^*_{off,i}$. The engagement of clutches decreases the actin flow rate, allowing the assembly of the actin microfilaments and, consequently, the spreading of the cell. Bangasser and Odde (42) demonstrated that the average dynamics of a motor-clutch model is able to describe experimental evidence, such as stiffness sensitivity of living cells. For this reason, a master equation-based analysis was performed and the MATLAB ODE solver was used to solve the equations governing the model (see *SI Appendix* for more details about the model in its canonical form). In the following, the clutch ensemble equations for our model are presented, making the assumption that the individual clutch values of bound probability, force, position, and off-rate can be substituted for their average values. Under this hypothesis, the change of the mean proportion of clutches bound in the ensemble (P_b) is

$$\frac{dP_b}{dt} = (1 - P_b)k_{on} - P_b\langle k^*_{off}\rangle. \quad [3]$$

The average force in the clutch is related to the extension in the clutch through the clutch spring constant, assumed equal for all of the clutches, k_c:

$$\langle F_c\rangle = k_c(\langle x_c\rangle - x_s), \quad [4]$$

where x_s is the substrate position and indicates one end of the clutch and $\langle x_c\rangle$ is the average position of the other end of the clutch.

The relationship between the substrate position x_s and the average position of the clutch $\langle x_c\rangle$ is calculated by writing the equilibrium equation between the clutch ensemble force, the substrate force, which is the sum of the contribution of the 2 springs, and the external force F_0, which generates the initial deformation, here indicated as x_0:

$$F_0 + n_c\langle F_c\rangle = F_s, \quad [5]$$

where

$$F_0 = k_s x_0 + k_s\frac{\sqrt{l^2 + x_0^2} - l}{\sqrt{l^2 + x_0^2}}x_0 \quad [6]$$

and

$$F_s = k_s x_s + k_s\frac{\sqrt{l^2 + x_s^2} - l}{\sqrt{l^2 + x_s^2}}x_s. \quad [7]$$

Combining Eqs. **3**–**5**, the relationship between x_s and $\langle x_c\rangle$ is the following:

$$\langle x_c\rangle = \frac{k_s + n_c k_c}{n_c k_c}x_s - \frac{k_s}{n_c k_c}x_0 + \frac{k_s}{n_c k_c}\left(1 - \frac{l}{\sqrt{l^2 + x_s^2}}\right)x_s - \frac{k_s}{n_c k_c}\left(1 - \frac{l}{\sqrt{l^2 + x_o^2}}\right)x_0. \quad [8]$$

The Hill equation (42) relates the retrograde flow rate to the force F_s:

$$v_f = v_u\left(1 - \frac{F_s}{n_m F_m}\right), \quad [9]$$

where v_u is the free velocity of myosin motors, n_m is the number of myosin motors, and F_m is the stall force for the single motor. We have, here, substituted the substrate force F_s with the only component due to the action of motor clutches. Then, Eq. **7** becomes

$$v_f = v_u\left(1 - \frac{F_s - F_0}{n_m F_m}\right) = v_u\left\{1 - \frac{k_s}{n_m F_m}\left[2(x_s - x_0) + l\left(\frac{x_0}{\sqrt{l^2 + x_o^2}} - \frac{x_s}{\sqrt{l^2 + x_s^2}}\right)\right]\right\}. \quad [10]$$

The equation used for the average clutch off-rate is the following (39):

$$\langle k^*_{off}\rangle = (1 - P_b)k_{off} + P_b k_{off}\left(1 - \frac{\langle F_c\rangle}{rP_b F_b}\right)^{-r}. \quad [11]$$

Finally, the equation for the velocity of the end of the single clutch is

$$\frac{d\langle x_c\rangle}{dt} = (1 - P_b)\frac{dx_s}{dt} + P_b v_f. \quad [12]$$

The velocity of the single clutch is a weighted average of the velocity of unbound clutches, equal to those of the substrate (dx_s/dt) and the velocity of bound clutches, equal to the actin flow rate (v_f). By using Eqs. **8** and **10**, Eq. **12** becomes

$$\frac{dx_s}{dt} = P_b v_u\left[1 - \frac{k_s}{n_m F_m}\left(2x_s - 2x_0 + \frac{x_0 l}{\sqrt{l^2 + x_o^2}} - \frac{x_s l}{\sqrt{l^2 + x_s^2}}\right)\right] \Big/ (1 - P_b)\frac{dx_s}{dt} + P_b v_f. \quad [13]$$

Statistical Analysis. Data are reported as mean ± SEM. Statistical comparisons were performed with a Student's unpaired test. P values of <0.05 denote statistically significant difference.

ACKNOWLEDGMENTS. We thank Professor Michele Russo (University of Naples) for his constructive advice on clutch model modification; Professor Sergio Savino, Dr. Giuseppe Scherillo, and Dr. Chiara Cosenza (University of Naples) for useful discussion on the model implementation; Professor Nicola Fusco (University of Naples) for his useful considerations on mathematical aspects of the clutch model; Professor Giovanni Filippone and Maria Laura Lo Gatto (University of Naples) for the extensional rheology measurements; and Dr. Oreste Leone for mechanical design.

1. V. Vogel, M. Sheetz, Local force and geometry sensing regulate cell functions. *Nat. Rev. Mol. Cell Biol.* **7**, 265–275 (2006).
2. F. Guilak *et al.*, Control of stem cell fate by physical interactions with the extracellular matrix. *Cell Stem Cell* **5**, 17–26 (2009).
3. C. C. DuFort, M. J. Paszek, V. M. Weaver, Balancing forces: Architectural control of mechanotransduction. *Nat. Rev. Mol. Cell Biol.* **12**, 308–319 (2011).
4. B. Martinac, Mechanosensitive ion channels: Molecules of mechanotransduction. *J. Cell Sci.* **117**, 2449–2460 (2004).
5. J. Y.-J. Shyy, S. Chien, Role of integrins in endothelial mechanosensing of shear stress. *Circ. Res.* **91**, 769–775 (2002).
6. D. Ingber, Integrins as mechanochemical transducers. *Curr. Opin. Cell Biol.* **3**, 841–848 (1991).
7. T. Kobayashi, M. Sokabe, Sensing substrate rigidity by mechanosensitive ion channels with stress fibers and focal adhesions. *Curr. Opin. Cell Biol.* **22**, 669–676 (2010).
8. B. Geiger, A. Bershadsky, R. Pankov, K. M. Yamada, Transmembrane crosstalk between the extracellular matrix–cytoskeleton crosstalk. *Nat. Rev. Mol. Cell Biol.* **2**, 793–805 (2001).
9. A. J. Engler, S. Sen, H. L. Sweeney, D. E. Discher, Matrix elasticity directs stem cell lineage specification. *Cell* **126**, 677–689 (2006).
10. O. Chaudhuri *et al.*, Hydrogels with tunable stress relaxation regulate stem cell fate and activity. *Nat. Mater.* **15**, 326–334 (2016).
11. N. Wang, J. D. Tytell, D. E. Ingber, Mechanotransduction at a distance: Mechanically coupling the extracellular matrix with the nucleus. *Nat. Rev. Mol. Cell Biol.* **10**, 75–82 (2009).
12. P. L. McNeil, Cellular and molecular adaptations to injurious mechanical stress. *Trends Cell Biol.* **3**, 302–307 (1993).
13. P. L. McNeil, R. A. Steinhardt, Loss, restoration, and maintenance of plasma membrane integrity. *J. Cell Biol.* **137**, 1–4 (1997).
14. M. Glogauer *et al.*, The role of actin-binding protein 280 in integrin-dependent mechanoprotection. *J. Biol. Chem.* **273**, 1689–1698 (1998).
15. A. M. Malek, S. Izumo, Mechanism of endothelial cell shape change and cytoskeletal remodeling in response to fluid shear stress. *J. Cell Sci.* **109**, 713–726 (1996).
16. M. Glogauer *et al.*, Calcium ions and tyrosine phosphorylation interact coordinately with actin to regulate cytoprotective responses to stretching. *J. Cell Sci.* **110**, 11–21 (1997).
17. M. Sato, K. Nagayama, N. Kataoka, M. Sasaki, K. Hane, Local mechanical properties measured by atomic force microscopy for cultured bovine endothelial cells exposed to shear stress. *J. Biomech.* **33**, 127–135 (2000).
18. X. Trepat *et al.*, Effect of stretch on structural integrity and micromechanics of human alveolar epithelial cell monolayers exposed to thrombin. *Am. J. Physiol. Lung Cell. Mol. Physiol.* **290**, L1104–L1110 (2006).
19. B. A. Smith, B. Tolloczko, J. G. Martin, P. Grütter, Probing the viscoelastic behavior of cultured airway smooth muscle cells with atomic force microscopy: Stiffening induced by contractile agonist. *Biophys. J.* **88**, 2994–3007 (2005).
20. S. W. Crowder, V. Leonardo, T. Whittaker, P. Papathanasiou, M. M. Stevens, Material cues as potent regulators of epigenetics and stem cell function. *Cell Stem Cell* **18**, 39–52 (2016).
21. K. Naruse, MECHANOMEDICINE: Applications of mechanobiology to medical sciences and next-generation medical technologies. *J. Smooth Muscle Res.* **54**, 83–90 (2018).
22. R. De, A. Zemel, S. A. Safran, Do cells sense stress or strain? Measurement of cellular orientation can provide a clue. *Biophys. J.* **94**, L29–L31 (2008).

23. A. K. Yip *et al*., Cellular response to substrate rigidity is governed by either stress or strain. *Biophys. J.* **104**, 19–29 (2013).
24. B. Chen, B. Ji, H. Gao, Modeling active mechanosensing in cell–matrix interactions. *Annu. Rev. Biophys.* **44**, 1–32 (2015).
25. A. Macdonald, A. R. Horwitz, D. A. Lauffenburger, Kinetic model for lamellipodal actin-integrin 'clutch' dynamics. *Cell Adhes. Migr.* **2**, 95–105 (2008).
26. C. E. Chan, D. J. Odde, Traction dynamics of filopodia on compliant substrates. *Science* **322**, 1687–1691 (2008).
27. B. L. Bangasser, S. S. Rosenfeld, D. J. Odde, Determinants of maximal force transmission in a motor-clutch model of cell traction in a compliant microenvironment. *Biophys. J.* **105**, 581–592 (2013).
28. A. Elosegui-Artola, X. Trepat, P. Roca-Cusachs, Control of mechanotransduction by molecular clutch dynamics. *Trends Cell Biol.* **28**, 356–367 (2018).
29. A. Elosegui-Artola *et al*., Mechanical regulation of a molecular clutch defines force transmission and transduction in response to matrix rigidity. *Nat. Cell Biol.* **18**, 540–548 (2016).
30. H. T. Nia *et al*., Solid stress and elastic energy as measures of tumour mechanopathology. *Nat. Biomed. Eng.* **1**, 0004 (2016).
31. M. A. Wozniak, C. S. Chen, Mechanotransduction in development: A growing role for contractility. *Nat. Rev. Mol. Cell Biol.* **10**, 34–43 (2009).
32. J. Dervaux, M. Ben Amar, Morphogenesis of growing soft tissues. *Phys. Rev. Lett.* **101**, 068101 (2008).
33. S. Fusco, V. Panzetta, V. Embrione, P. A. Netti, Crosstalk between focal adhesions and material mechanical properties governs cell mechanics and functions. *Acta Biomater.* **23**, 63–71 (2015).
34. V. Panzetta *et al*., X-rays effects on cytoskeleton mechanics of healthy and tumor cells. *Cytoskeleton (Hoboken)* **74**, 40–52 (2017).
35. T. Mizutani, H. Haga, K. Kawabata, Cellular stiffness response to external deformation: Tensional homeostasis in a single fibroblast. *Cell Motil. Cytoskeleton* **59**, 242–248 (2004).
36. F. Chowdhury *et al*., Material properties of the cell dictate stress-induced spreading and differentiation in embryonic stem cells. *Nat. Mater.* **9**, 82–88 (2010).
37. M. Aragona *et al*., A mechanical checkpoint controls multicellular growth through YAP/TAZ regulation by actin-processing factors. *Cell* **154**, 1047–1059 (2013).
38. S. Kumar *et al*., Viscoelastic retraction of single living stress fibers and its impact on cell shape, cytoskeletal organization, and extracellular matrix mechanics. *Biophys. J.* **90**, 3762–3773 (2006).
39. S. Dupont *et al*., Role of YAP/TAZ in mechanotransduction. *Nature* **474**, 179–183 (2011).
40. S. Fusco, V. Panzetta, P. A. Netti, Mechanosensing of substrate stiffness regulates focal adhesions dynamics in cell. *Meccanica* **52**, 3389–3398 (2017).
41. V. Panzetta *et al*., ECM mechano-sensing regulates cytoskeleton assembly and receptor-mediated endocytosis of nanoparticles. *ACS Biomater. Sci. Eng.* **3**, 1586–1594 (2017).
42. B. L. Bangasser, D. J. Odde, Master equation-based analysis of a motor-clutch model for cell traction force. *Cell. Mol. Bioeng.* **6**, 449–459 (2013).
43. I. Johnston, D. McCluskey, C. Tan, M. Tracey, Mechanical characterization of bulk Sylgard 184 for microfluidics and microengineering. *J. Micromech. Microeng.* **24**, 035017 (2014).
44. S. Zhao *et al*., Mechanical stretch for tunable wetting from topological PDMS film. *Soft Matter* **9**, 4236–4240 (2013).
45. A. Einstein, On the motion of small particles suspended in liquids at rest required by the molecular-kinetic theory of heat. *Annalen der Physik* **17**, 549–560 (1905).
46. Y. Tseng, T. P. Kole, D. Wirtz, Micromechanical mapping of live cells by multiple-particle-tracking microrheology. *Biophys. J.* **83**, 3162–3176 (2002).
47. T. M. Squires, T. G. Mason, Fluid mechanics of microrheology. *Annu. Rev. Fluid Mech.* **42**, 413–438 (2009).
48. Y. Tseng, T. P. Kole, S.-H. J. Lee, D. Wirtz, Local dynamics and viscoelastic properties of cell biological systems. *Curr. Opin. Colloid Interface Sci.* **7**, 210–217 (2002).
49. C. P. Brangwynne, G. H. Koenderink, F. C. MacKintosh, D. A. Weitz, Intracellular transport by active diffusion. *Trends Cell Biol.* **19**, 423–427 (2009).
50. B. D. Hoffman, G. Massiera, K. M. Van Citters, J. C. Crocker, The consensus mechanics of cultured mammalian cells. *Proc. Natl. Acad. Sci. U.S.A.* **103**, 10259–10264 (2006).
51. N. Gal, D. Lechtman-Goldstein, D. Weihs, Particle tracking in living cells: A review of the mean square displacement method and beyond. *Rheol. Acta* **52**, 425–443 (2013).